Nanoscale

Accepted Manuscript

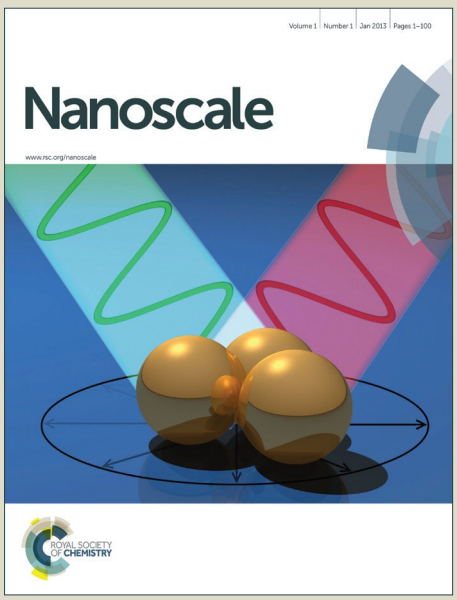

ROYAL SOCIETY OF CHEMISTRY

www.rsc.org/nanoscale

the junction have been mapped through scanning tunneling spectroscopy (STS), their charge separation ability has been studied by forming hybrid bulk-heterojunction solar cells with the heterodimers in a suitable polymer matrix.

2 Experimental

A Formation of CdS|CdTe heterodimers

CdS|CdTe heterodimers were synthesized following a reported route.[10] Briefly, for the synthesis of CdS nanoparticles in their wurtzite phase, 0.25 mmol $CdCl_2 \cdot H_2O$ (52.2 mg), 2.5 mmol (0.8 mL) oleic acid, and 10 mL dioctyl ether were mixed and degassed for 10 min at 120 °C. The solution was then heated to 220 °C at which 0.25 mmol of sulfur stock solution in 0.8 mL oleylamine was swiftly injected into the reaction flux. The reaction was allowed to continue for 10 min to allow formation of CdS nanostructures. The reaction was stopped by lowering temperature of the flask down to room temperature; the nanostructures were washed and separated through re-dispersion in hexane and precipitation with hexane and ethanol in sequence.

To form CdS|CdTe heterodimers, CdS nanostructures were allowed to undergo an anion exchange process to form zinc-blende structure of CdTe. To do so, CdS nanostructures dispersed in 4 mL of oleylamine were heated to 260 °C under an inert environment. TOP:Te solution containing 1.2 mL TOP (trioctylphosphine) and 0.3 mmol tellurium (Te) was swiftly injected to the reaction flask. Anionic exchange process occurred at this temperature resulting in formation of CdS|CdTe heterodimer. Instead of core-shell nanostructures, a heterodimer between CdS and CdTe formed so that the strain due to mismatch of their lattices remains to a minimum. Since the reaction time determined the extent of the exchange process, we collected the nanostructures after 20, 60, 90, and finally 120 min after injection of the tellurium complex. Within 120 min, we anticipated a complete replacement of sulfur in forming CdTe nanostructures. The nanostructures were washed in ethanol and redispersed in hexane for further characterization.

B Characterization of CdS|CdTe heterodimers

The nanostructures were characterized through optical absorption spectroscopy, X-ray diffraction (XRD) studies, transmission electron microscopy (TEM), high-resolution TEM (HR-TEM), dark-field and scanning TEM (STEM) images, and X−ray photoelectron spectroscopy (XPS). The instruments used in this regard were Shimadzu UV−2550 Spectrophotometer, a Bruker D8 Advanced X−ray Powder Diffractometer, a JEM 2100F Jeol TEM, and an XPS instrument (Omicron: serial no. 0571), respectively. Individual nanoparticles and heterodimers were characterized in an ultrahigh vacuum scanning tunneling microscope (PAN style UHV-STM of M/s RHK Technology, Inc.). To record the image of individual nanostructures and their STS, their ultra-dilute solutions were drop-casted on freshly-cleaved (through a scotch-tape method) highly ordered pyrolytic graphite (HOPG). While the STM chamber was under a pressure of 2×10^{-10} Torr, temperature of the substrate and the tungsten tip both were kept at 100 K. During approach of the tip, a current of 0.1 nA was targeted to achieve at 2.0 V. For smoothing of STM topographies, WSxM software was used. We considered electron-tunneling to have occurred through a double barrier tunnel junction (DBTJ).[28] To avoid tip-induced band bending effect (TIBB) and also maintain DBTJ, we chose a low-current during the approach of the tip, so that charge accumulation effect was minimum at the tip-semiconductor interface.[29]

C Device fabrication and characterization

Solar cells were fabricated on semitransparent indium tin oxide (ITO) electrodes, which were stripped and had a surface resistance of 15 Ω/square. Poly(3,4-ethylenedioxythiophene) polystyrenesulfonate (PEDOT:PSS) solution was spun on the electrodes followed by annealing at 120 °C for 20 min to form a hole-collecting layer. The ITO substrates coated with a PEDOT:PSS layer, the heterodimers, ZnO nanoparticles formed through a conventional sol-gel synthesis route, and electronic-grade poly(3-hexylthiophene-2,5-diyl) (P3HT), which was purchased from Rieke Metals, LLC., Lincoln, were then transferred to a glove box to continue with the film formation process. The P3HT was head-to-tail regioregular (91-94 %) and had an average molecular weight (M_w) of 50,000-70,000. To form an active layer of hybrid bulk-heterojunction (BHJ), P3HT and the heterodimers at a measured ratio (10:8, 10:1, or 10:0.5 by weight) were added to chloroform to form a solution having a concentration of 15 mg/mL. The solution was spun on the PEDOT:PSS film at 2000 rpm for 30 s to form an active layer of the hybrid BHJ devices. Apart from the three heterodimers that were formed as a result of the anionic exchange reaction for 20, 60, and 90 min, CdS and CdTe nanostructures were also added to P3HT separately to form thin-films P3HT:CdS and P3HT:CdTe hybrid BHJ. After annealing the films at 150 °C within the glove-box, ZnO nanoparticles in 1-butanol solution was spun to form an electron-collecting layer followed by further annealing at 120 °C. Strips of aluminum were then thermally evaporated under a vacuum in a evaporation chamber attached to the glove-box. Area of the devices, as resulted from overlap of ITO and the aluminum strips orthogonal to each other, was 6 mm^2.

The devices were characterized inside the glovebox that had an upright solar simulator as an attachment. A Newport-Stratfort 300 W Solar Simulator, located outside the glovebox, provided the simulated solar illumination to the devices. A Keithley 2636A Electrometer was used to measure current-voltage (*I–V*) characteristics of the devices in dark and illumination conditions. A mask was used to ensure that the areas outside the cell did not receive any light during the measurements.

3 Result and discussion

A Characterization of the heterodimers

We have recorded optical absorption spectra of different heterodimers that were formed by varying reaction time of the anionic exchange process. The spectra, as presented in Fig. 1, show a continuum in the high-energy region that is characteristic to such II-VI semiconductors. The spectra in addition showed an increase in NIR-component when the time of reaction increased leading to formation of CdTe through an anionic exchange process. It appears from the spectra that the exchange process or formation of CdTe was complete at a reaction time of 120 min.

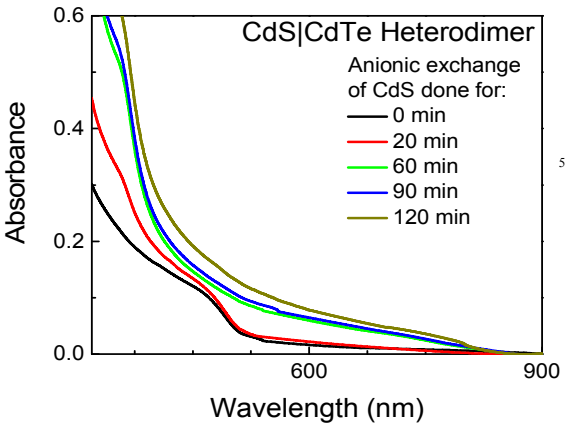

Fig. 1 Optical absorption spectra of CdS, CdTe, and different CdS|CdTe heterodimers.

XRD patterns of CdS and CdTe nanostructures and different CdS|CdTe heterodimers are shown in Fig. 2. The peaks of CdS could be indexed to their wurtzite (space group P63mc) phase when compared with Joint Committee on Powder Diffraction Standards (JCPDS) file #041-1049. Similarly, the pattern of CdTe could be indexed to their zinc-blende phase when compared with JCPDS file #033-0490. In the spectra of CdS|CdTe heterodimers, most of the peaks of the two crystalline materials could be found to be present. Intensity of the peaks corresponding to the two materials expectedly depended on the extent of anion exchange process, that is, on the content of each of the materials in the heterodimers.

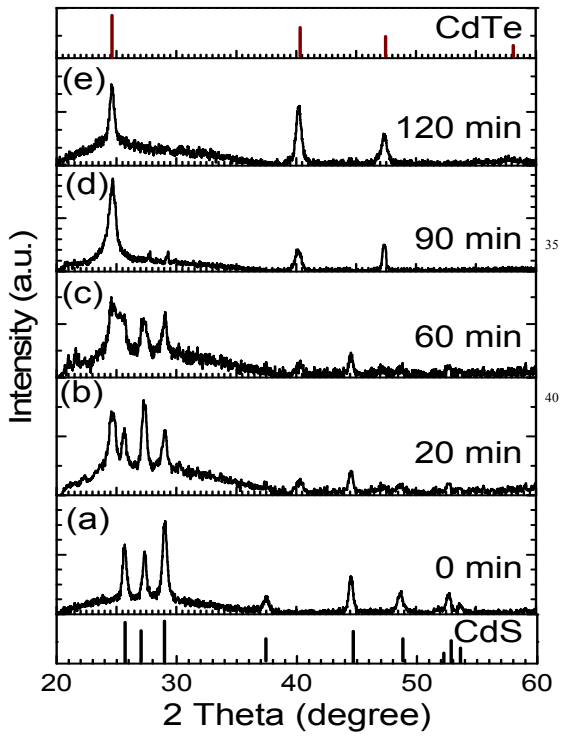

Fig. 2 XRD patterns of CdS nanostructures after anionic exchange reaction of (a) 0, (b) 20, (c) 60, (d) 90, and (e) 120 min in forming CdS|CdTe heterodimers. Patterns from JCPDS files for the CdS and the CdTe crystals are shown with sticks at the two extreme X-axes of the plot.

TEM and HR-TEM images of CdS and CdTe nanostructures and of CdS|CdTe heterodimers are shown in Fig. 3. The images show that the average diameter of CdS nanostructures was about 13 nm. Upon anionic exchange, cadmium from the surface of CdS participated in forming CdS|CdTe heterodimer. HR-TEM images of the heterodimers show that the interface was clearly separated by the two regions. The images moreover brought out two lattice-separations confirming presence of two materials in the nanostructures. An interlayer spacing of 0.336 and 0.345 nm at the two sections of the heterodimers matched well with the {002} plane of wurtzite-CdS and the {100} plane of zinc-blende CdTe, respectively. The images of CdS and CdTe nanostructures expectedly exhibited planes of only one single crystal. The STEM images of heterodimers, as shown in Fig. 3, also confirmed the presence of two materials in the heterostructures. When the anion-exchange process was carried out for a short time (20 min), the CdTe section was much smaller than the CdS one; with exciton Bohr radius of CdTe being 7 nm, such CdS|CdTe heterodimers can hence be termed as a combination of bulk and quantum dot phases. As the reaction time grew (60 min), both the semiconductors attained their bulk phase. At still longer reaction times (90 min), the size of CdS left in the heterodimer shrunk down to around 3.5–4.0 nm. Again, with exciton Bohr radius of CdS being 3.5 nm, such CdS|CdTe heterodimers can be termed as a combination of quantum dot and bulk phases. We therefore could form three types of CdS|CdTe heterodimers, namely bulk|dot, bulk|bulk, and dot|bulk.

The progress of growth of heterodimers could be visualized in the histogram of size of the two semiconductors (Fig. 3C). As the reaction time elapsed, the size of CdS section decreased. The average size of CdTe, as observed in the histogram, similarly increased evidencing formation of bulk|dot, bulk|bulk, and dot|bulk heterodimers in sequence.

We have recorded XPS spectra of CdS and CdTe nanoparticles and different CdS|CdTe heterodimers. The spectrum of CdS brought out typical binding energies corresponding to 3d, 3p, and 4s, states of cadmium and 2s and 2p of sulfur;[30,31] the spectrum of CdTe similarly exhibited 3d, 4s, and 4p of tellurium apart from the above-mentioned states of cadmium.[32] XPS spectrum of heterodimers having a typical content of CdS and CdTe are shown in Fig. S1†. The energies obtained in XPS analysis were corrected with respect to C1s peak at 284.5 eV.

The binding energies in the XPS analysis show peaks that corresponded to 3p and 3d states of Cd^{2+}, 3d state of Te^{2-}, and 2s and 2p states of S^{2-} inferring formation of $Cd^{2+}S^{2-}$ and $Cd^{2+}Te^{2-}$ in the nano-heterojunctions. The states of the elements were further identified by recording high-resolution spectra in designated energy regions (Fig. S1†). For example, Cd 3p resolved into $3p_{1/2}$ and $3p_{3/2}$ appearing at 652.0 and 617.9 eV, respectively. Similarly, peaks at 410.6 and 403.9 eV matched well with the $3d_{3/2}$ and $3d_{5/2}$ states, respectively, of the reported spectrum of cadmium. The peaks at 225.2 and 160.6 eV could be referenced to 2s and $2p_{3/2}$ states of sulfur, respectively. Finally the 3d states of tellurium occurred at 573.0 and 583.0 eV, which could be identified to $3d_{3/2}$ and $3d_{5/2}$ state of the element, respectively.

B Scanning tunneling spectroscopy and band positions of heterodimers

The heterodimers could also be visualized in STM topographies.

Typical topographies of CdS nanostructures after anionic exchange reaction of (a) 0, (b) 20, (c) 60, (d) 90, and (e) 120 min are shown in Fig. 4. With a set-point of 0.1 nA at 2.0 V applied to the substrate, the tip in effect probed current through electron-injection to the conduction band of the semiconductors. As we stated earlier, while two extremes reaction-times represent CdS and CdTe nanostructures, the intermediate ones resulted CdS|CdTe heterodimers having different extent of the components, namely bulk|dot, bulk|bulk, and dot|bulk junctions. The topographies matched well with their corresponding TEM images. Color contrast of the two materials did not resolve in the topographics since the tip-to-material height contributes to tunneling current exponentially; a mapping along the junction in a constant current mode therefore led to a little height difference in the topographies. The size obtained in the topographies was slightly higher than that observed in HR-TEM images, since electronic wave-function of the nanostructures were mapped by probing the conduction-band of the nanostructure that can often extend out of physical boundaries of the materials. Finite curvature of the tip could also lead to an increased size in the STM topographies.

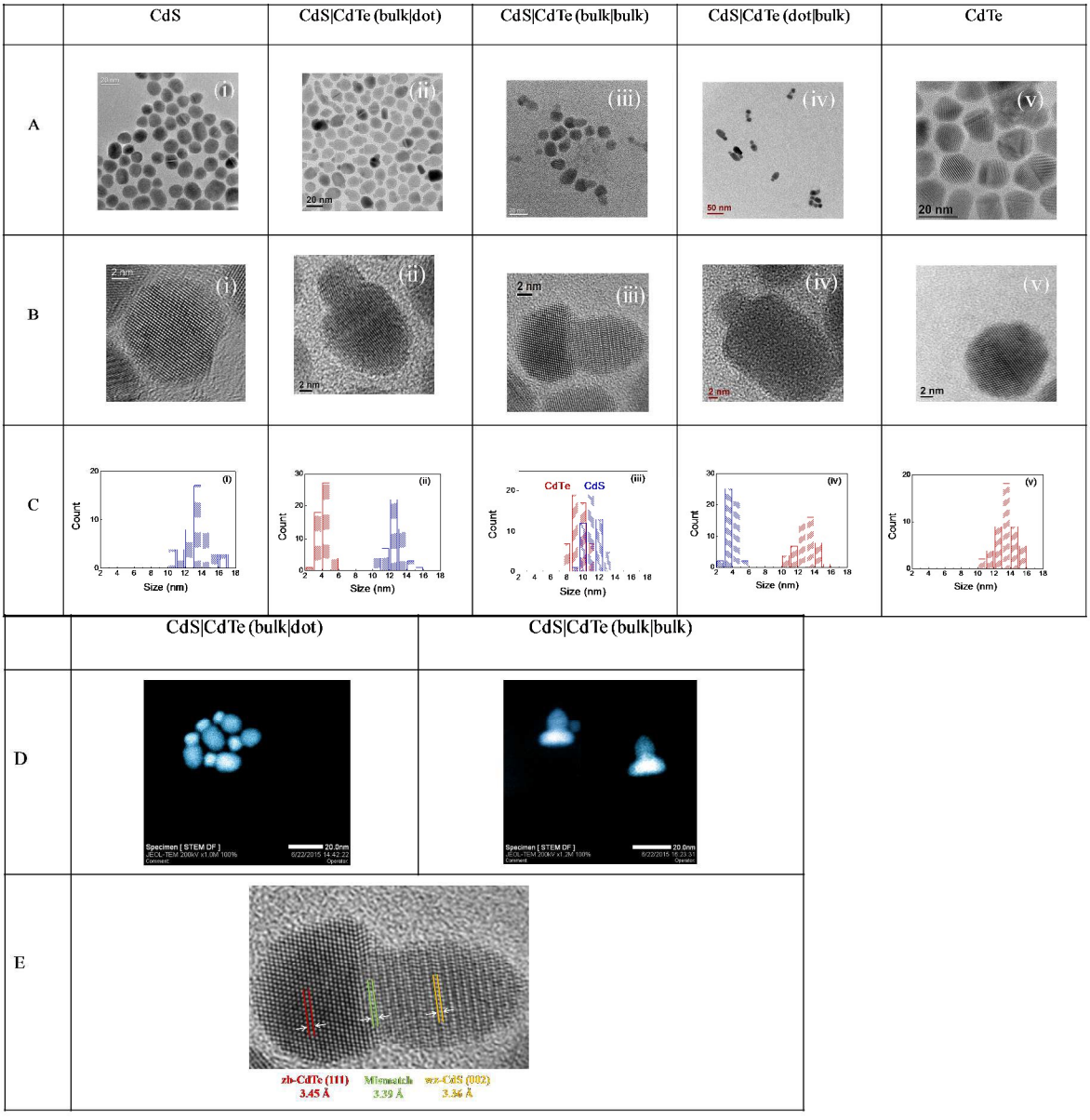

Fig 3 (A) TEM and (B) HR-TEM images of CdS nanostructures after anionic exchange reaction of (i) 0, (ii) 20, (iii) 60, (iv) 90, and (v) 120 min. While two extremes represent CdS and CdTe nanoparticles, the intermediate reaction-times resulted CdS|CdTe heterodimers having different extent of the components. (C) Histogram of size of CdS and CdTe sections in the nanostructures/heterodimers as the anionic exchange process progressed. (D) STEM images of two types of heterodimers. (E) A HR-TEM image of a typical CdS|CdTe heterodimer showing lattice planes of the semiconductor-nanocrystals.

Cite this: DOI: 10.1039/c0xx00000x

www.rsc.org/xxxxxx

ARTICLE TYPE

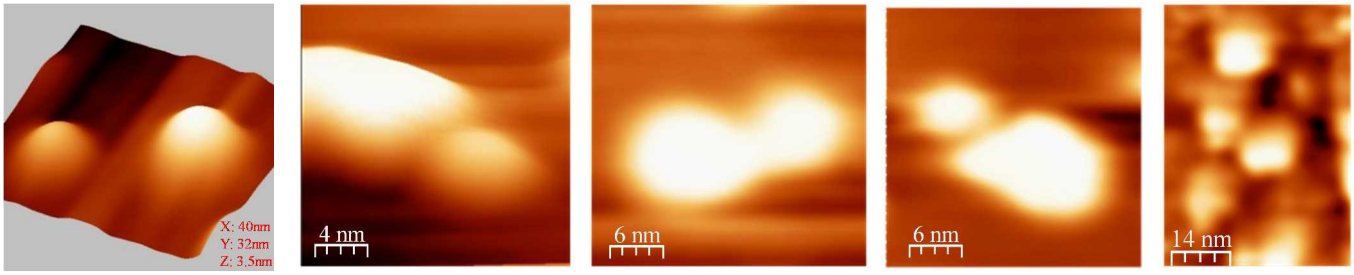

Fig 4 STM topographies of CdS nanostructures after anionic exchange reaction of (a) 0, (b) 20, (c) 60, (d) 90, and (e) 120 min (from left to right). The images were recorded with a set-point of 0.1 nA at 2.0 V applied to the substrate.

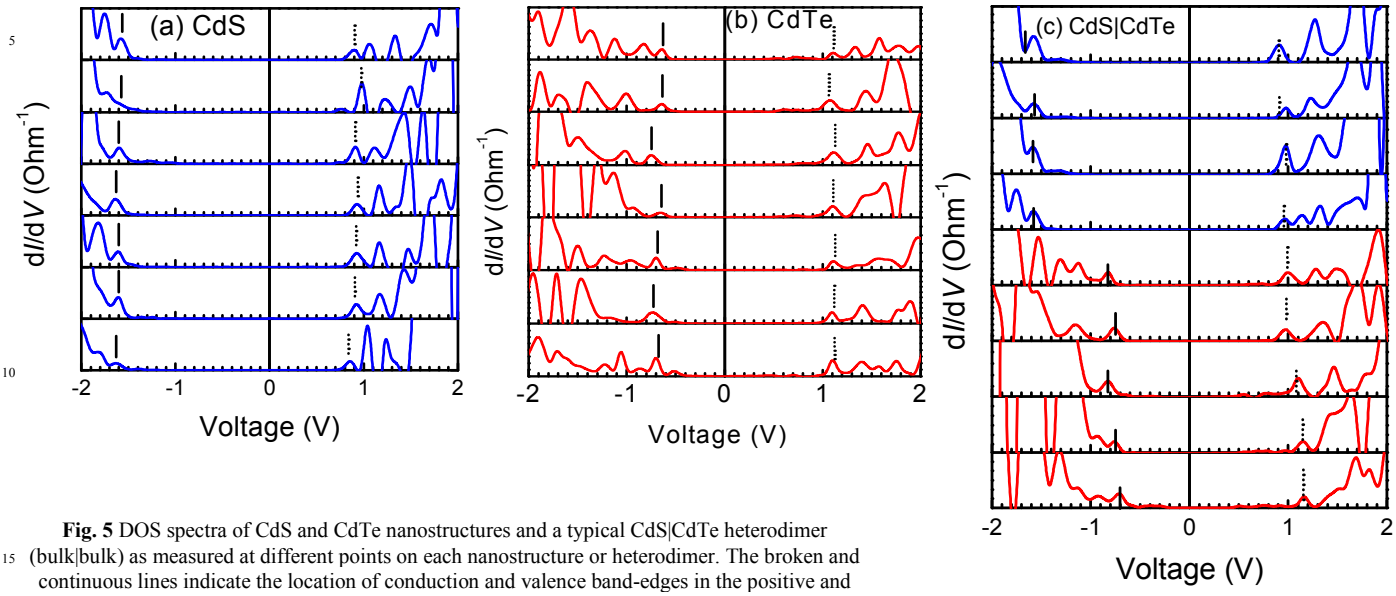

Fig. 5 DOS spectra of CdS and CdTe nanostructures and a typical CdS|CdTe heterodimer (bulk|bulk) as measured at different points on each nanostructure or heterodimer. The broken and continuous lines indicate the location of conduction and valence band-edges in the positive and negative voltage, respectively.

The scanning tunneling spectroscopy was recorded after disabling the feedback-loop. From the tunneling current, we determined differential conductance (dI/dV) that has correspondence to the density of states (DOS) of the materials. This enabled us to locate the CB and VB edges of the semiconductors with respect to their Fermi energy. For STM measurements, since the voltage was applied to the HOPG substrate, the peaks in the negative voltage of DOS spectrum denoted the VB of the semiconductors. Similarly, the peaks at positive voltages, at which electrons could be injected to the nanostructures, provided the location of the CB.

The dI/dV – V characteristics of CdS and CdTe nanostructures and a typical heterodimer are shown in Fig. 5. In each nanostructure, the spectra were recorded at many different points on the structure. The CB and VB energies are also identified in each DOS spectrum. With the energies being located with respect to the Fermi energy, the DOS spectrum of CdS evidenced that the Fermi energy was closer to the CB edge inferring *n*-type nature of the semiconductor. Similarly, the DOS spectra of CdTe brought out *p*-type nature of the binary semiconductor.

The STS spectra across a *pn*-junction in general bring out *p*- and *n*-sections along with depletion region at the interface.[26] When we look at the spectra of a CdS|CdTe heterodimer at which both have bulk-behavior (Fig. 5c), we observed CB and VB of CdS and CdTe at the two ends. The band-edges can be found to undergo a shift near the interface evidencing existence of a depletion region. The spectra of bulk|dot and dot|bulk CdS|CdTe heterodimers (Fig. S2†) moreover bring out signature of quantum-confined dot phases having atomic-like states.[22,33] Since we recorded STS along the three different CdS|CdTe heterodimers in their bulk|dot, bulk|bulk, and dot|bulk configurations, we summed up their band-energies in Fig. 6. The points at which differential conductance were recorded are marked on the topographies of the respective heterodimers. The results show that a controlled formation of *pn*-junction in a nanostructure was achieved. The images moreover brought out the depletion region in the junction. The depletion region in these three heterodimers had different widths; while the dot section was

mostly fully-depleted, the semiconductor when in the bulk form was depleted only near the junction. The dot being fully-depleted, the width of depletion region in bulk|dot and dot|bulk heterodimers turned out to be shorter than that could have formed between CdS and CdTe semiconductor nanostructures, that is, the bulk|bulk case. The bulk|bulk heterodimers had the widest depletion region (13 nm) which extended to both the semiconductors; apart from the depletion region, the bulk|bulk heterodimer contained both *p*- and *n*-sections at the two ends of the nanostructure. In a following, we will show how the width (of the depletion region) controls charge separation process through a drift of minority carriers across the region and hence the photovoltaic performance.

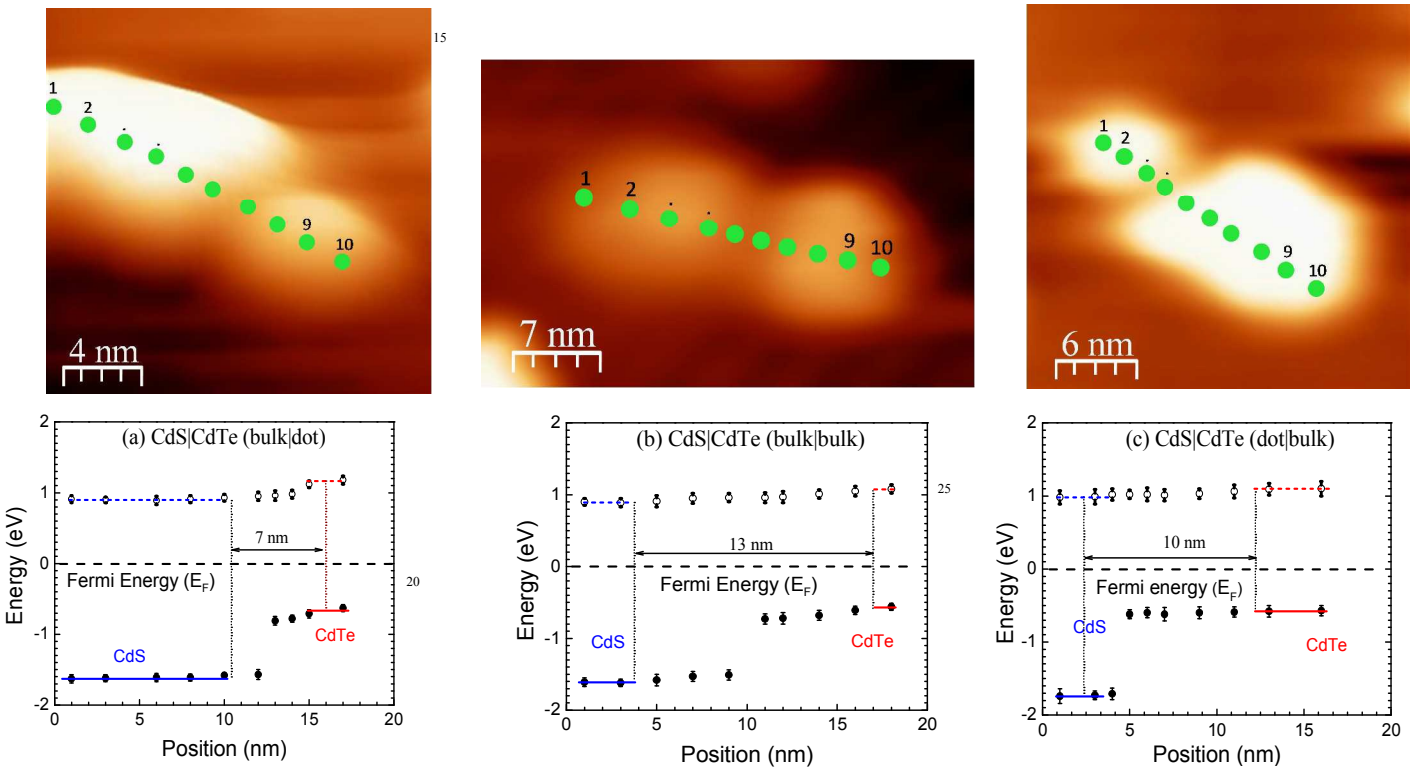

Fig. 6 Band-mapping of three different CdS|CdTe heterodimers formed after anionic exchange reaction of CdS nanostructures for (a) 20, (b) 60, and (c) 90 min. The figures in addition show the STM topography of the nanorod junctions and the spots at which tunneling current was measured. Points marked as 1 through 10 in the topographies represent CB and VB edges from left to right in each figure. Fermi energy (E_F) across the junction and the depletion region of the heterodimers are also shown in each of the figures. On each point on a heterodimer, at least five dI/dV – V characteristics were recorded to determine the CB and VB edges. The five measurements at each point have been summed up as error bars in energy values.

C dI/dV imaging of CdS|CdTe heterodimers in their CB and VB

We also recorded dI/dV images of the heterodimer at selected positive and negative voltages. As we stated earlier, a negative voltage would imply probing of VB of the dimer. Since the magnitude would determine the semiconductor(s) that would be tapped, we varied the voltage. In Fig. 7, we show dI/dV images of a heterodimer biased at -0.7 and -1.65 V. We observe that at a low voltage (0.7 V), the tip could tap only the CdTe section of the heterodimer, since no states of CdS were available at such a bias. At a higher voltage magnitude (-1.65 V), states of both the semiconductors were available making both the semiconductors visible in the dI/dV image. Similarly, when the CB was probed with a positive voltage, CdS section could be imaged at a low voltage (0.95 V). Here, no states of CdTe were available at such a voltage. At higher biases (1.15 V), both the semiconductors could be visible in the dI/dV imaging.

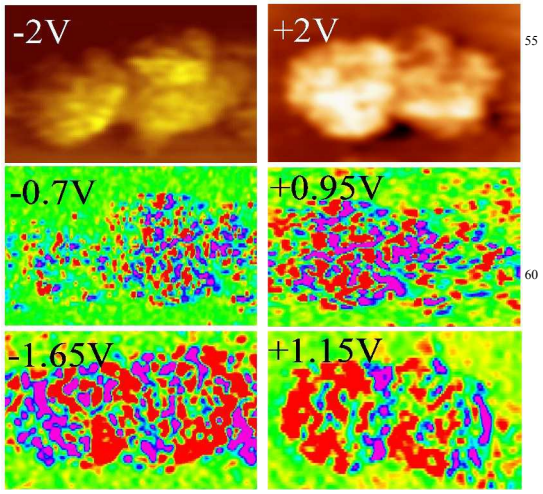

Fig. 7 dI/dV imaging of a CdS|CdTe heterodimer recorded at different biases using lock-in amplifier (12 mV rms 782 Hz). While negative voltages probed VB of the dimer, positive voltages probed the CB. STM topographies of the dimer by recording its CB and VB are shown in the upper panel.

D Photoinduced charge separation and photovoltaic properties

With a *pn*-junction being formed in each of the CdS|CdTe heterodimers and each junction containing a depletion region, we studied their charge-separation properties. The heterodimers would separate carriers efficiently due to type-II band-alignment at the interface. In order to study their charge-separating ability, we formed sandwiched structures with BHJ between the heterodimers and P3HT as an active layer. We expected that the output of hybrid BHJ solar cells would have a correspondence with the charge-separation ability of the heterodimers. We may add here that a sharp interface would facilitate formation of the depletion region and would also widen the region. Alloying or formation of a mixed phase at the interface may adversely affect photo-induced charge separation process.

We have formed devices based on (thin-films of) hybrid BHJ of the nanostructures in a polymer matrix sandwiched between ITO and aluminum electrodes. Here, the nanostructures used in forming the hybrid BHJs were CdS, three different CdS|CdTe heterodimers, and finally CdTe nanostructures. Schematic diagram of a device structure is shown in the inset of Fig. 8. *I–V* characteristics of the devices under a dark condition are shown in Fig. 8(a). The characteristics were rectifying in nature which was due to the dissimilar work-function of ITO and aluminum used in forming the sandwiched structures.

When we characterized the devices under a white illumination, all the devices acted as solar cells (Fig. 8b). As we compare the characteristics, we find that performance of the devices based on heterodimers were better than that with CdS or with CdTe nanostructures. Since we also varied the content of the nanostructures in the polymer, we enlisted parameters of all the solar cells in Table 1. We observe that for any weight ratio, the devices with heterodimers returned better photovoltaic parameters as compared to the individual nanostructures, all in the polymer matrix.

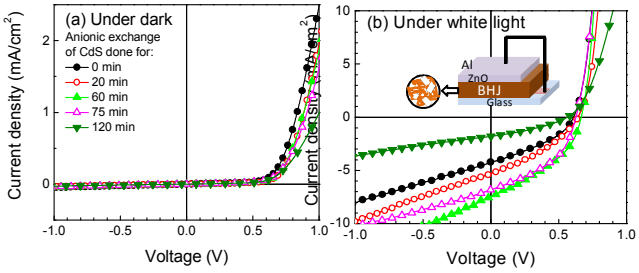

Fig. 8 Current-voltage characteristics of hybrid BHJ solar cells based on CdS nanostructures after anionic exchange reaction of 0, 20, 60, 90, and 120 min in P3HT matrix under (a) dark and (b) 1 Sun illumination condition. While the two extremes represent CdS and CdTe nanostructures, the intermediate reaction-times resulted CdS|CdTe heterodimers having different extent of the components. Schematic diagram of a device structure is shown in the inset of (b).

Table 1. Open-circuit voltage (V_{OC} in V), short-circuit current (I_{SC} in mA/cm^2), fill-factor (FF in percent), and energy conversion efficiency (η in percent) of different hybrid BHJ solar cells containing CdS and CdTe nanostructures and different CdS|CdTe heterodimers; content of the nanostructures in the polymer matrix that has also been varied, is stated in the table.

Reaction time of CdS (Nanostructure in P3HT)	Nanostructure:P3HT ratio											
	5 weight%				10 weight%				80 weight%			
	V_{OC}	I_{SC}	FF	η	V_{OC}	I_{SC}	FF	η	V_{OC}	I_{SC}	FF	η
0 min (CdS)	0.63	0.14	27	0.023	0.62	0.34	30	0.063	0.61	4.2	28	0.72
20 min (CdS|CdTe) (bulk|dot)	0.62	0.16	26	0.026	0.63	0.36	28	0.065	0.64	5.3	31	1.06
60 min (CdS|CdTe) (bulk|bulk)	0.66	0.18	32	0.038	0.67	0.38	34	0.086	0.68	7.5	36	1.84
90 min (CdS|CdTe) (dot|bulk)	0.62	0.15	29	0.028	0.63	0.35	32	0.071	0.63	6.8	34	1.60
120 min (CdTe)	0.58	0.04	22	0.005	0.60	0.11	25	0.016	0.58	1.8	22	0.32

As such, improved performance in the BHJs based on heterodimers is due to introduction of an efficient channel for charge separation in the form of depletion region at CdS|CdTe heterodimers. We have observed that the I_{SC} and accordingly solar cell efficiency was higher in BHJs based on bulk|bulk heterodimers as compared those based on bulk|dot or dot|bulk ones. As we inferred earlier, the width of depletion region was wider in the former heterodimer as compared to the latter ones. The results hence implied that the width of depletion region had a direct influence on solar cell performance which primarily depended on the ability of charge separation since the quantum of photoabsorption and routes of carrier transport remained the same in these devices.

If we look at different parameters of solar cells, such as V_{OC}, I_{SC}, and fill-factor, we observe that all of them improved in the bulk|bulk heterodimer based BHJs as compared to those with bulk|dot or dot|bulk ones. The V_{OC}, which depends on band-offsets of the components and is affected by recombination of carriers in the devices, optimized in bulk|bulk heterodimer based BHJs. That is, a wider depletion region separates carriers to a longer extent leading to lesser recombination loss, which correspondingly yielded an improvement in the fill-factor of bulk|bulk heterodimer based hybrid BHJ devices.

We may also add that in varying the weight ratio between the nanostructures and the polymer, a lower concentration of the nanostructures was chosen to sift the effect of charge separation ability of the heterodimers on solar cell parameters minimizing the variation of photoabsorption that the nanostructures introduce

when their concentration was higher (80 weight%). The results based on 10 and 5 weight% of nanostructures in the polymer also bring out the importance of the use of bulk|bulk heterodimers as compared to the other two CdS|CdTe dimers and the individual semiconductor nanostructures.

4 Conclusions

In conclusion, we have grown CdS|CdTe heterodimers through a partial anionic exchange process. By varying the reaction time, we could form different heterodimers with the semiconductor components evidencing bulk|dot, bulk|bulk, and dot|bulk forms in the junction. Since the two semiconductors form a type-II band-alignment at their interface, a depletion region formed in the heterodimers that led to separation of charge carriers. From scanning tunneling spectroscopy and correspondingly the density of state, we mapped the band-edges along the nanostructure and the heterodimers; we have observed that the width of depletion region depended on the reaction time in forming CdTe in the dimers. When one of the components of dimers is in the quantum confinement region, the smaller material became fully-depleted leading to shrinkage in the width of depletion region. We have observed that when diameters of both the components are over the quantum confinement limit, the width of depletion region maximized. Charge separation ability of the heterodimers studied in hybrid BHJ solar cells based on such nanostructures corresponded with the width of depletion region.

Acknowledgements

The authors acknowledge Mr. Supriya Chakraborty for his contribution for recording TEM images. They also acknowledge financial assistance from DeitY, SERIIUS, and Nano Mission (DST) projects. AB acknowledges CSIR Fellowship Nos. 09/080(0779)/2011-EMR-I (Roll No. 510847).

†Electronic supplementary information (ESI) available: See DOI: 10.1039/c0xx00000x

References

1 D. Lee, M. F. Rubner and R. E. Cohen, *Nano Lett.*, 2006, **6**, 2305-2312.
2 B. Pradhan, S. K. Batabyal and A. J. Pal, *Appl. Phys. Lett.*, 2006, **89**, 233109.
3 S. Blankenburg, J. M. Cai, P. Ruffieux, R. Jaafar, D. Passerone, X. L. Feng, K. Mullen, R. Fasel and C. A. Pignedoli, *ACS Nano*, 2012, **6**, 2020-2025.
4 G. H. Li, A. Sundararajan, A. Mouti, Y. J. Chang, A. R. Lupini, S. J. Pennycook, D. R. Strachan and B. S. Guiton, *Nanoscale*, 2013, **5**, 2259-2263.
5 J. M. Cai, C. A. Pignedoli, L. Talirz, P. Ruffieux, H. Sode, L. B. Liang, V. Meunier, R. Berger, R. J. Li, X. L. Feng, K. Mullen and R. Fasel, *Nat. Nanotechnol.*, 2014, **9**, 896-900.
6 B. Sadtler, D. O. Demchenko, H. Zheng, S. M. Hughes, M. G. Merkle, U. Dahmen, L. W. Wang and A. P. Alivisatos, *J. Am. Chem. Soc.*, 2009, **131**, 5285-5293.
7 H. B. Li, R. Brescia, M. Povia, M. Prato, G. Bertoni, L. Manna and I. Moreels, *J. Am. Chem. Soc.*, 2013, **135**, 12270-12278.
8 C. S. Tan, C. H. Hsiao, S. C. Wang, P. H. Liu, M. Y. Lu, M. H. Huang, H. Ouyang and L. J. Chen, *ACS Nano*, 2014, **8**, 9422-9426.
9 J. Park, H. Zheng, Y.-W. Jun and A. P. Alivisatos, *J. Am. Chem. Soc.*, 2009, **131**, 13943-13945.
10 M. Saruyama, Y. G. So, K. Kimoto, S. Taguchi, Y. Kanemitsu and T. Teranishi, *J. Am. Chem. Soc.*, 2011, **133**, 17598-17601.
11 J. Debgupta, R. Devarapalli, S. Rahman, M. V. Shelke and V. K. Pillai, *Nanoscale*, 2014, **6**, 9148-9156.
12 D. V. Talapin, R. Koeppe, S. Gotzinger, A. Kornowski, J. M. Lupton, A. L. Rogach, O. Benson, J. Feldmann and H. Weller, *Nano Lett.*, 2003, **3**, 1677-1681.
13 H. M. Zhu, N. H. Song and T. Q. Lian, *J. Am. Chem. Soc.*, 2010, **132**, 15038-15045.
14 G. Rainò, T. Stoferle, I. Moreels, R. Gomes, Z. Hens and R. F. Mahrt, *ACS Nano*, 2012, **6**, 1979-1987.
15 S. Kim, B. Fisher, H. J. Eisler and M. Bawendi, *J. Am. Chem. Soc.*, 2003, **125**, 11466-11467.
16 T. Teranishi and M. Sakamoto, *J. Phys. Chem. Lett.*, 2013, **4**, 2867-2873.
17 M. Okano, M. Sakamoto, T. Teranishi and Y. Kanemitsu, *J. Phys. Chem. Lett.*, 2014, **5**, 2951-2956.
18 M. Sakamoto, K. Inoue, M. Saruyama, Y. G. So, K. Kimoto, M. Okano, Y. Kanemitsu and T. Teranishi, *Chem. Sci.*, 2014, **5**, 3831-3835.
19 H. M. Zhu and T. Q. Lian, *Energy Environ. Sci.*, 2012, **5**, 9406-9418.
20 U. Dasgupta, A. Bera and A. J. Pal, *Sol. Energy Mater. Sol. Cells*, 2015, **143**, 319-325.
21 Z. L. Chen, H. Zhang, Q. S. Zeng, Y. Wang, D. D. Xu, L. Wang, H. Y. Wang and B. Yang, *Adv. Energy Mater.*, 2014, **4**, 1400235.
22 B. Alperson, I. Rubinstein, G. Hodes, D. Porath and O. Millo, *Appl. Phys. Lett.*, 1999, **75**, 1751-1753.
23 U. Banin, Y. W. Cao, D. Katz and O. Millo, *Nature*, 1999, **400**, 542-544.
24 D. Steiner, D. Dorfs, U. Banin, F. Della Sala, L. Manna and O. Millo, *Nano Lett.*, 2008, **8**, 2954-2958.
25 Y. L. Wang, Y. P. Jiang, M. Chen, Z. Li, C. L. Song, L. L. Wang, K. He, X. Chen, X. C. Ma and Q. K. Xue, *J. Phys.-Condes. Matter*, 2012, **24**, 475604.
26 A. Bera, S. Dey and A. J. Pal, *Nano Lett.*, 2014, **14**, 2000-2005.
27 S. U. Nanayakkara, J. van de Lagemaat and J. M. Luther, *Chem. Rev.*, 2015, **115**, 8157-8181.
28 U. Banin and O. Millo, *Annu. Rev. Phys. Chem.*, 2003, **54**, 465-492.
29 R. M. Feenstra, Y. Dong, M. P. Semtsiv and W. T. Masselink, *Nanotechnology*, 2007, **18**, 044015.
30 E. C. Hao, H. P. Sun, Z. Zhou, J. Q. Liu, B. Yang and J. C. Shen, *Chem. Mater.*, 1999, **11**, 3096-3102.
31 T. Nakanishi, B. Ohtani and K. Uosaki, *J. Phys. Chem. B*, 1998, **102**, 1571-1577.
32 H. Borchert, D. V. Talapin, N. Gaponik, C. McGinley, S. Adam, A. Lobo, T. Moller and H. Weller, *J. Phys. Chem. B*, 2003, **107**, 9662-9668.
33 B. Diaconescu, L. A. Padilha, P. Nagpal, B. S. Swartzentruber and V. I. Klimov, *Phys. Rev. Lett.*, 2013, **110**, 127406.

Cite this: DOI: 10.1039/c0xx00000x

www.rsc.org/xxxxxx

ARTICLE TYPE

ToC Graphics

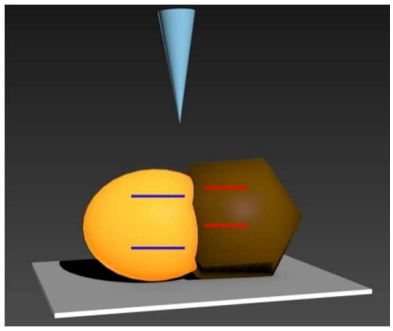

ToC Text

With a control over the duration of anionic exchange process, bulk|dot, bulk|bulk, and dot|bulk phases of CdS|CdTe heterodimers were formed. The depletion region, which was found to depend on the phase of the semiconductors from scanning tunneling spectroscopy, had a direct correlation with the photoinduced charge separation process in the heterodimers.